Laser Channeling in Millimeter-Scale Underdense Plasmas of Fast-Ignition Targets

Ignition in inertial confinement fusion (ICF) starts in a hot spot in the core of compressed fuel pellets. In conventional ICF schemes, the hot spot—a small region with a temperature of ~10 keV—is created through a highly symmetric compression driven by multiple laser beams that illuminate the target from all directions.[1] In fast ignition (FI) a separate ignition pulse is used to create the hot spot after the core has been compressed, thereby relaxing symmetry requirements and leading to higher gain.[2] There are several scenarios for getting the ignition pulse close to the compressed core. In the so-called "hole-boring" scenario of FI, the ignition pulse is to first propagate through a millimeter (mm)-scale underdense plasma to reach a critical surface with a critical density $n_c = \omega_0^2 m_e \big/ (4\pi e^2)$ (m_e and e are electron mass and charge, respectively, and ω_0 is the pulse frequency). There the ignition pulse may continue to push forward into the overdense plasma through its ponderomotive pressure (hole boring) and relativistic transparency. As the intense laser interacts with the overdense plasma, it generates energetic electrons that must eventually reach the dense core region where their energy is to be absorbed to create the hot spot. An alternative way to move the ignition pulse closer to the core region is to use fuel pellets with a hollow gold cone attached to one side. The compression beams illuminate the target from all directions except those within the opening of the cone. The asymmetric compression still leads to a dense core and has the potential to lead to a clear path for the ignition pulse to propagate up to a very overdense plasma. The first integrated FI experiments with the coned targets showed a 10^3 times fusion neutron increase.[3] However, the hole-boring scenario is still being actively pursued for its more symmetric compression and its absence of radiation loss associated with the gold cone.

Many factors affect the overall efficiency of converting the ignition pulse energy to the hot-spot energy, including the conversion efficiency to the energetic electrons at the critical surface,[4–6] the angular spread of these electrons,[7,8] and the slowing-down and scattering of the electrons as they propagate to the core.[9] Of particular concern to the hole-boring scenario is the loss of ignition pulse energy through laser–plasma interactions in the mm-scale underdense plasma.[10] While a small-amplitude electromagnetic wave can linearly propagate through densities less than n_c without much loss, the petawatt (PW) ignition pulse can interact with the plasma in a highly nonlinear manner, leading to processes such as laser self-focusing[11,12] and filamentation,[13,14] as well as scattering[15] and significant plasma heating and density modification.[14,16] Energy lost in this region will not be available for hole boring and energetic electron generation at the critical surface. A channeling pulse, which could be the prepulse of the ignition pulse or a separate pulse, has been proposed[2] to produce a low-density channel to reduce the nonlinear interactions of the ignition pulse in the underdense region. Plasma density channels were created using lasers with intensities of $I = 10^{17}$ to 10^{19} W/cm^2 in experiments of laser–solid target or laser–gas jet interactions.[17–20] Increased transmission of a trailing $I = 10^{20}$ W/cm^2 in the density channel was also observed.[19] Two dimensional (2-D) and three-dimensional (3-D) particle-in-cell (PIC) simulations of these experiments showed laser self-focusing in the plasma and channel generation through the ponderomotive force and resulting shock expansion.[18,21,22] Most of these previous experiments and simulations were done in 100-μm-scale plasmas.

The underdense region of an actual FI target, however, is about 1000 μm long. The residual plasma in the channel can continue to interact with the latter part of the channeling pulse and the ignition pulse. Later stages of the nonlinear evolution of the pulses and the channel need to be studied with full spatial scale simulations to obtain values of critical parameters such as the channeling time (T_c) and the required channeling pulse energy (E_c) and their scaling with the laser intensity I. These are needed to assess the viability of the hole-boring scheme and to plan for integrated experiments on next-generation FI facilities. This article presents results from 2-D PIC simulations with the code *OSIRIS*[23] showing that channeling in mm-scale plasmas is a highly nonlinear and dynamic process involving laser self-focusing and filamentation, channel generation via shock waves, longitudinal plasma snowplowing, laser hosing, and channel bifurcation and self-correction. As a result, the channeling speed oscillates and is much less than the laser

linear group velocity. We find that it eventually asymptotes to the expression obtained by conservation of momentum even for densities less than the critical density.

In our 2-D PIC simulations, a channeling pulse of wavelength λ_0 is launched from the left boundary of the simulation box with a peak intensity between $I = 10^{18}$ and 10^{20} $(1\ \mu\text{m}/\lambda_0)^2$ W/cm^2 and a rise time of 150 laser periods, after which the pulse amplitude is kept constant. The transverse profile is Gaussian with a full-width-at-half-maximum intensity spot size of $r_0 = 16$ to 47 λ_0 ($1/e$ spot size for the electric field, $w_0 = 90$ to 264 c/ω_0). It is focused onto a surface 600 λ_0 away from the left boundary. Both s- and p-polarizations are used to infer 3-D effects. The initial plasma density profile used is $n_0 = 0.1\ n_c \exp(x/L)$ with $L = 430\ \lambda_0$. (Length and time in these simulations are normalized to λ_0 and $1/\omega_0$, respectively, but $\lambda_0 = 1\ \mu$m is assumed so that the density scale length L is comparable to that of FI targets.) The ion-to-electron mass ratio is $m_i/m_e = 4590$, thereby approximating a DT plasma. The electron and ion temperatures are $T_e = T_i = 1$ keV. We simulate the region of $n_0 = 0.1$ to $1.02\ n_c$ ($x = 0$ to 1000 λ_0) in two different setups. In the first setup we simulate the whole region in two separate simulations, one for $n_0 = 0.1$ to $0.3\ n_c$ and the other for $n_0 = 0.3$ to $1\ n_c$. The simulation box size is $L_x = 477\ \lambda_0$ (longitudinal) and $L_y = 262\ \lambda_0$ (transverse) for the low-density portion and $L_x = 523\ \lambda_0$ and $L_y = 262\ \lambda_0$ for the high-density portion. The grid resolution in these simulations is $\Delta_x = 0.314\ c/\omega_0$ and $\Delta_y = 0.628\ c/\omega_0$. Ten particles per cell are used for each species in this setup. In the second setup we simulate the entire region in one simulation with a box size of $L_x = 987\ \lambda_0$ and $L_y = 401\ \lambda_0$ (totaling 19740×4010 cells). The grid resolution is kept the same but one particle per cell is used for each species.

We now describe general features of the channeling process using results from a simulation where $I = 10^{19}$ W/cm^2, $r_0 = 16\ \mu$m, and the laser was p-polarized. Other simulations with different intensities and/or with an s-polarized laser display similar features. The channeling pulse power P greatly exceeds the power threshold for relativistic self-focusing P_c (Ref. 4). For $n/n_c = 0.1$, $P/P_c = 300\ P/(10^{12}\ \text{W})$ $n/n_c \approx 780 \gg 1$ and r_0 is $32\ c/\omega_p$. Therefore, relativistic whole-beam self-focusing and filamentation of the pulse[5] occur before significant plasma density perturbations arise. This initial phase is dominated by filamentation that is seeded by the Gaussian transverse profile since the initial r_0 is $32\ c/\omega_p$ [Fig. 112.20(a)]. As the laser self-focuses and filaments, the laser normalized vector potential a within each filament increases and the radius of each filament decreases. This causes the transverse ponderomotive force from each filament to increase so that significant electron density depletion occurs.[5] The space charge force ultimately causes the ions to follow, leading to the formation of several microdensity channels, with $n_{\max}/n_{\min} \approx 6$ [Fig. 112.20(b)].

Due to the fact that the microdensity channels form at different times along the laser propagation direction, the walls of the channels develop a longitudinal modulation. As new laser energy flows straight toward the filaments, the ponderomotive forces snowplow away the microchannels, eventually destroying them. This leads to the merging of neighboring mini-channels, eventually forming a single density channel centered along the axis of the laser [Fig. 112.20(c)]. At the end of this stage, a high-mach-number ion-acoustic shock is launched, causing the walls of the channel to move radially outward at a fairly constant speed of 0.03 c. The channel eventually becomes much wider than r_0.

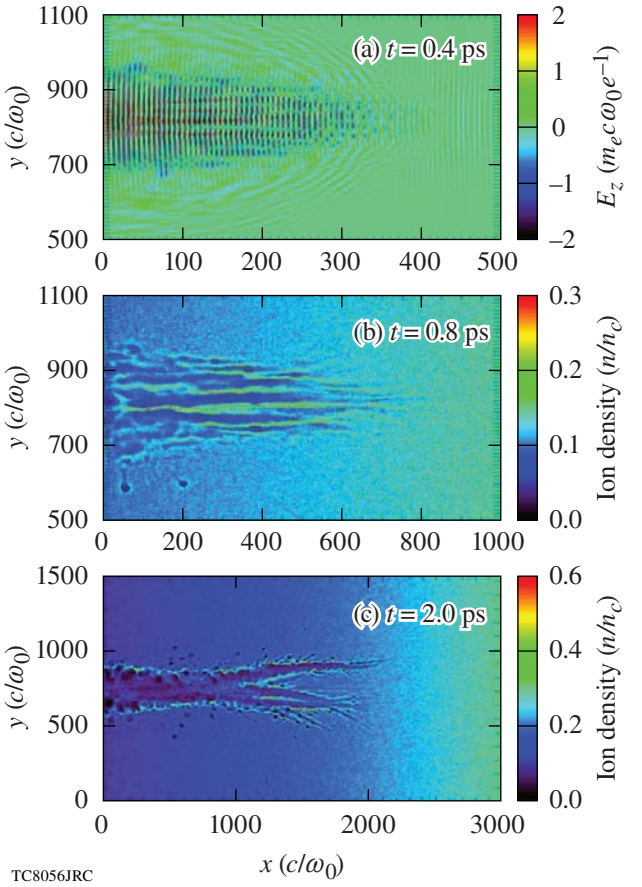

Figure 112.20
Results from a simulation with an $I = 10^{19}$ W/cm^2, p-polarized laser and $n_0 = 0.1$ to $0.3\ n_c$. (a) Laser E-field at $t = 0.4$ ps showing relativistic self-focusing and filamentation; (b) ion density at $t = 0.8$ ps showing the formation of microchannels; (c) ion density at $t = 2.0$ ps showing the formation of a single channel at the center for $x < 1000\ c/\omega_0$.

This entire process repeats as the laser and the head of the channel gradually advance toward the critical surface. Additionally, at the head of the channel, the density piles up to a value several times the local value of the initial density (Fig. 112.21). The density buildup grows as the channel digs into higher density. At regions of $n_0 > 0.55\ n_c$, the density compression exceeds n_c [Fig. 112.21(b)], thus making the subsequent pulse propagation similar to the hole-boring process, slower than the linear group velocity for the initial local density $v_g \equiv \sqrt{1 - n_0/n_c}$. While the transverse expansion is regular, the advance of the head of the channel is dynamic and intermittent. The channel can bend away from its center due to a long-wavelength hosing instability. This is seeded by hosing the head of the laser on the electron time scale as it propagates up the density gradient. For a finite-width pulse in a uniform plasma, the hosing instability[24] is caused by upward or downward tilting of local wavefronts due to a transverse phase velocity difference across the wavefronts. The phase velocity gradient is caused by the plasma density perturbation driven by the ponderomotive force of the hosing pulse.[25] The channel bends because of the hosing pulse, whose first occurrence is at $t \approx 3$ ps in the simulation with $n_0 = 0.1$ to $0.3\ n_c$ [Fig. 112.22(a)]. With the initial pulse parameters $a = 2.7$, $w = 90\ c/\omega_0$, and observed $k_h = (\pi/500)\ \omega_0/c$, the predicted growth rate in the long-wavelength regime,[25,26] $\gamma_{hu} = \left(a/\sqrt{8}\right)(c/\omega_0 w)k_h c \approx 0.13\ \text{ps}^{-1}$ may seem too slow for this observed time. However, self-focusing makes a larger and w smaller than their initial values and can increase γ_h. There is another channel-bending instability caused by the plasma pressure, but its growth rate $\gamma_{hp} \sim C_{sk_h} \sim 0.07\ \text{ps}^{-1}$ (Ref. 27) is too small even for $T_e = 1$ MeV.

As the channel hoses, the radius of curvature gradually increases. At some point the curvature becomes too severe to trap all of the incoming energy. As a consequence, some of

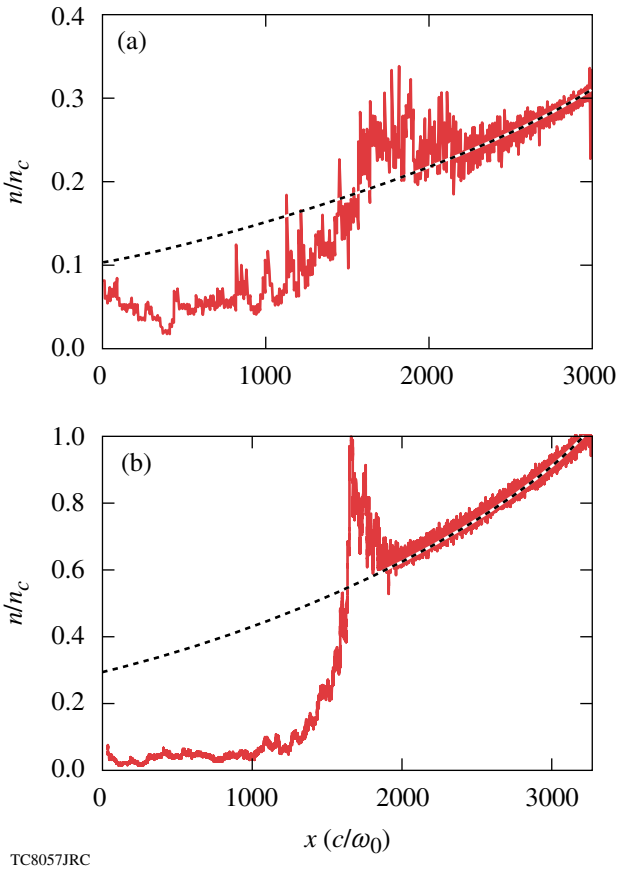

Figure 112.21
Average channel density plots for (a) $n_0 = 0.1$ to $0.3\ n_c$ at $t = 8.2$ ps and (b) $n_0 = 0.3$ to $1.0\ n_c$ at $t = 8$ ps showing the density pile-up. The dotted lines are the initial density profiles.

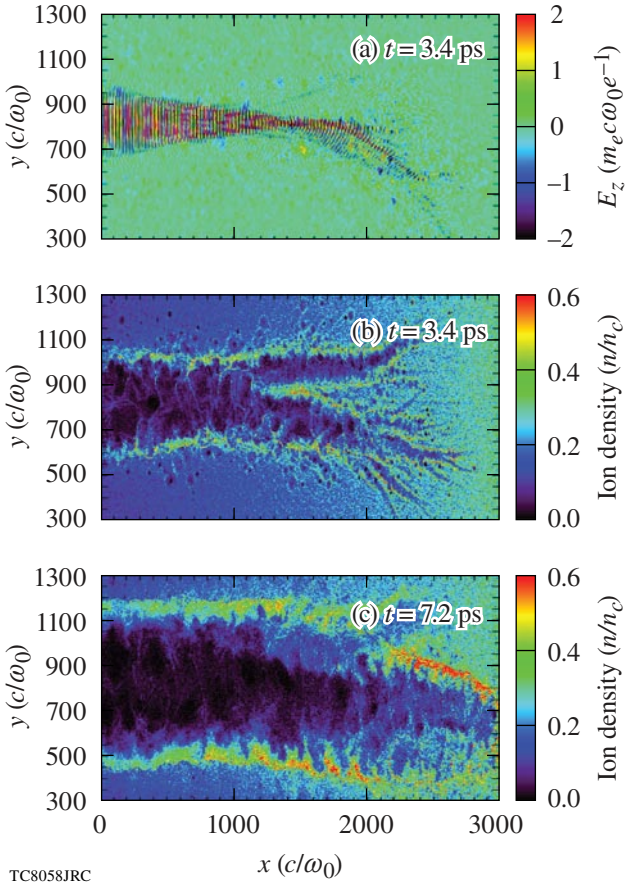

Figure 112.22
Results from a simulation with an $I = 10^{19}$ W/cm^2, p-polarized laser and $n_0 = 0.1$ to $0.3\ n_c$. (a) Laser E-field showing laser hosing; (b) ion density showing channel bifurcation at $t = 3.4$ ps; (c) ion density at $t = 7.2$ ps showing channel self-correction.

the laser energy breaks out of the channel to form a second branch of the channel that bends in the opposite direction. This process stalls the channel formation process. Both branches then advance deeper into the plasma, leaving a narrow plasma "island" in the middle of the entire channel [Fig. 112.22(b)]. Eventually, the island is pushed away by the ponderomotive force of the incoming laser energy and the two branches merge to form again a single channel [Fig. 112.22(c)]. This process of bifurcation and self-correction can repeat in a simulation lasting ~10 ps and provides a mechanism for the head of the channel to advance in propagation caused by the hosing-bending instability. Over time, the channel direction remains along the pulse propagation direction in our simulations.

Residual densities in the channel vary for different pulse intensities, from 0.1 n_c for $I = 10^{18}$ W/cm^2 to 0.04 n_c for $I = 10^{20}$ W/cm^2. To determine T_c, the time needed for the channel to reach the critical surface, under different pulse intensities, we define the channel as any location where the average plasma density is less than $n_r = 0.1\ n_c$. The average density, rather than the lowest density, in the channel is more relevant for the transmission of the ignition pulse. Specifically, the density is averaged transversely around the pulse center y_c, $y_c - w/2 < y < y_c + w/2$. The channel front X_c is defined as the location when the average density decreases to n_r and the channel advance speed is defined as $v_c = \mathrm{d}X_c/\mathrm{d}t$. Figure 112.23 plots the time for the channel to reach different density surfaces for three pulse intensities, measured from the one-particle-per-cell and p-polarization runs, and the resulting v_c for the $I = 10^{19}$ W/cm^2 case. It shows that v_c generally decreases as n_0 increases; however, v_c also oscillates as the channel advances, reflecting the underlying bifurcation and self-correction process seen in Figs. 112.22(b) and 112.22(c). We emphasize that v_c describes the speed of the density modification rather than the speed at which the laser energy advances. Figure 112.23(b) shows that v_c is much less than v_g and asymptotes to the ponderomotive hole-boring velocity [Eq. (1)]

$$v_{\mathrm{hb}} = 0.6\, c \sqrt{\frac{n_c}{n_0}\frac{m_e}{m_i}\frac{I\lambda_0^2}{10^{18}\ \mathrm{W}\mu\mathrm{m}^2/\mathrm{cm}^2}}\,, \tag{1}$$

as the front density buildup exceeds n_c. At the end of these simulations, the channel did not reach the critical surface. We estimate T_c by fitting and extrapolating the data in Fig. 112.23(a) and find T_c = 283, 72, and 15 ps for $I = 10^{18}$, 10^{19}, and 10^{20} W/cm^2, respectively. An intensity scaling can be found from this limited data set,

$$T_c \approx 2.9 \times 10^2 \left(I/10^{18}\ \mathrm{W/cm}^2\right)^{-0.64}\ \mathrm{ps}\,, \tag{2}$$

which enables us to obtain an intensity scaling for the total energy needed to reach the critical surface,

$$E_c \approx 1.7\left(I/10^{18}\ \mathrm{W/cm}^2\right)^{0.36}\ \mathrm{kJ}. \tag{3}$$

From this scaling we can see that the channeling pulse intensity should be kept as low as possible to minimize the total energy used in the channeling process. However, the ignition process needs to be completed within ~100 ps, which sets a lower bound for the channeling intensity to $I \approx 5 \times 10^{18}$ W/cm^2. If the self-focusing and other nonlinear interactions were neglected and channeling were taken to be the hole-boring process described

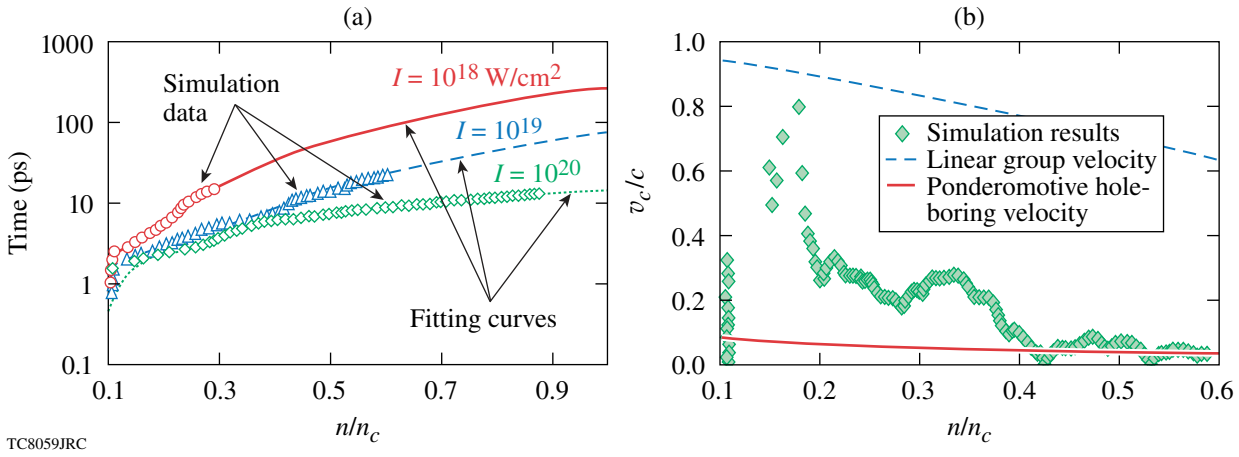

Figure 112.23
(a) Time for the channel to reach different initial densities under different pulse intensities and the corresponding fitting curves. Data were taken from the one-particle-per-cell and $n_0 = 0.1$ to 1.0 n_c runs. (b) The channeling speed v_c in the $I = 10^{19}$ W/cm^2 case.

by Eq. (1) from the beginning, analytical expressions for T_c and E_c can be obtained for density profiles dn/dx,

$$T_c^{(\mathrm{hb})} = \int \mathrm{d}n\left(\mathrm{d}n/\mathrm{d}x\right)^{-1}\Big/ v_{\mathrm{hb}} = 2.2 \times 10^2 \left(I\Big/10^{18}\ \mathrm{W}\Big/\mathrm{cm}^2\right)^{-0.5}\ \mathrm{ps},$$

and $E_c^{(\mathrm{hb})} \approx 1.3\left(I/10^{18}\ \mathrm{W/cm}^2\right)^{0.5}$ kJ for these simulations. That $T_c^{(\mathrm{hb})}$ and $E_c^{(\mathrm{hb})}$ are close to those from Eqs. (2) and (3) shows that despite the complexity of the channel formation, the channeling in these parameter regimes eventually becomes largely a ponderomotive process.

The scalings of Eqs. (2) and (3) are based on the available data set with p-polarization. The s-polarization data show a slightly larger v_c but similar scalings with intensities. The difference in v_c is due to less laser absorption in the channel walls in the s-polarization case than in the p-polarization case. In reality, the difference in the laser absorption at the channel walls in the directions perpendicular and parallel to the polarization may cause different expansion rates in the two directions, resulting in a noncircular channel cross section. In addition, self-focusing is stronger in 3-D than in 2-D, which may lead to a larger channeling speed in 3-D. These effects will be studied in future 3-D simulations with reduced scales; however, currently, full-scale 3-D simulations are not feasible even on the largest computers available.

In summary, channeling in the mm-scale underdense plasma of fast-ignition targets is a highly nonlinear and dynamic process. The channel expands transversely from density perturbations created by the relativistic and ponderomotive pulse self-focusing and filamentation. The density buildup near the channel front can eventually reach above the critical density, making the channeling speed much less than the linear group velocity of an electromagnetic wave. The channeling speed approaches estimates based on momentum conservation and 100% reflection of the laser at the density pile-up at the channel front[10] (although the second of these assumptions is not met). The scaling of the channeling time obtained from the PIC simulations indicates that a low-intensity channeling pulse is preferred to minimize the total channeling energy, but the intensity cannot be much lower than $I \approx 5 \times 10^{18}$ W/cm^2 if the channeling is to be completed within 100 ps. It is worth pointing out that for a typical fast-ignition target, the critical surface for 1-μm light will be roughly 600 μm in front of the target center. One way to move the channel closer to the core would be to use blue light ($\lambda = 0.35$ μm) for both the channeling and ignition pulses.

ACKNOWLEDGMENT

This work was supported by U.S. Department of Energy under Grants Nos. DE-FG02-06ER54879, DE-FC02-04ER54789, DE-FG52-06NA26195, and DE-FG02-03ER54721. Simulations were carried out at the National Energy Research Scientific Computing Center through an INCITE award and on the UCLA DAWSON Cluster under grant no. NSF-Phy-0321345. We wish to acknowledge useful discussions with Dr. R. Betti and Dr. W. Seka.

REFERENCES

1. J. D. Lindl, Phys. Plasmas **2**, 3933 (1995).
2. M. Tabak *et al*., Phys. Plasmas **1**, 1626 (1994).
3. R. Kodama *et al*., Nature **412**, 798 (2001); *ibid*. **418**, 933 (2002).
4. S. C. Wilks *et al*., Phys. Rev. Lett. **69**, 1383 (1992).
5. A. Pukhov and J. Meyer-ter-Vehn, Phys. Rev. Lett. **79**, 2686 (1997).
6. C. Ren *et al*., Phys. Rev. Lett. **93**, 185004 (2004).
7. C. Ren *et al*., Phys. Plasmas **13**, 056308 (2006).
8. J. C. Adam, A. Héron, and G. Laval, Phys. Rev. Lett. **97**, 205006 (2006).
9. C. K. Li and R. D. Petrasso, Phys. Rev. E **70**, 067401 (2004).
10. K-C. Tzeng, W. B. Mori, and C. D. Decker, Phys. Rev. Lett. **76**, 3332 (1996).
11. C. Max, J. Arons, and A. B. Langdon, Phys. Rev. Lett. **33**, 209 (1974).
12. G.-Z. Sun *et al*., Phys. Fluids **30**, 526 (1987).
13. P. Kaw, G. Schmidt, and T. Wilcox, Phys. Fluids **16**, 1522 (1973).
14. A. B. Langdon and B. F. Lasinski, Phys. Rev. Lett. **34**, 934 (1975).
15. D. W. Forslund, J. M. Kindel, and E. L. Lindman, Phys. Fluids **18**, 1002 (1975).
16. W. B. Mori *et al*., Phys. Rev. Lett. **60**, 1298 (1988).
17. M. Borghesi *et al*., Phys. Rev. Lett. **78**, 879 (1997).
18. J. Fuchs *et al*., Phys. Rev. Lett. **80**, 1658 (1998).
19. A. J. Mackinnon *et al*., Phys. Plasmas **6**, 2185 (1999).
20. K. A. Tanaka *et al*., Phys. Rev. E **60**, 3283 (1999).
21. A. Pukhov and J. Meyer-ter-Vehn, Phys. Rev. Lett. **76**, 3975 (1996).
22. Y. Sentoku *et al*., Fusion Sci. Technol. **49**, 278 (2006).
23. R. G. Hemker, "Particle-in-Cell Modeling of Plasma-Based Accelerators in Two and Three Dimensions," Ph.D. thesis, University of California, 2000; R. A. Fonseca, L. O. Silva, F. S. Tsung, V. K. Decyk, W. Lu, C. Ren, W. B. Mori, S. Deng, S. Lee, T. Katsouleas, and J. C. Adam, in *Computational Science—ICCS 2002*, edited by P. M. A. Sloot *et al*., Lecture Notes in Computer Science (Springer, Berlin, 2002), pp. 343–351.

24. G. Shvets and J. S. Wurtele, Phys. Rev. Lett. **73**, 3540 (1994); P. Sprangle, J. Krall, and E. Esarey, Phys. Rev. Lett. **73**, 3544 (1994).

25. C. Ren and W. B. Mori, Phys. Plasmas **8**, 3118 (2001).

26. B. J. Duda and W. B. Mori, Phys. Rev. B **61**, 1925 (2000); B. J. Duda *et al*., Phys. Rev. Lett. **83**, 1978 (1999).

27. E. Valeo, Phys. Fluids **17**, 1391 (1974).